# Strong-field- versus weak-field-ionization pump-probe spectroscopy

Spencer L. Horton, Yusong Liu, Pratip Chakraborty, Philipp Marquetand, Tamás Rozgonyi, Spiridoula Matsika, and Thomas Weinacht

Phys. Rev. A **98**, 053416 — Published 14 November 2018

DOI: 10.1103/PhysRevA.98.053416

# Strong-Field vs Weak-Field Ionization Pump-Probe Spectroscopy

Spencer L. Horton[1], Yusong Liu[1], Pratip Chakraborty[2], Philipp Marquetand[3], Tamás Rozgonyi[4,5], Spiridoula Matsika[2], and Thomas Weinacht[1]
[1] *Department of Physics and Astronomy, Stony Brook University, Stony Brook, NY 11794, USA*
[2] *Department of Chemistry, Temple University, Philadelphia, PA 19122, USA*
[3] *University of Vienna, Faculty of Chemistry, Institute of Theoretical Chemistry, Währinger Str. 17, 1090 Wien, Austria*
[4] *Institute of Materials and Environmental Chemistry, Research Centre for Natural Sciences, Hungarian Academy of Sciences, Budapest 1117 Magyar tudósok krt. 2, Hungary and*
[5] *Wigner Research Centre for Physics, Hungarian Academy of Sciences, P.O. Box 49, H-1525 Budapest, Hungary*

Ionization can serve as a universal probe of excited state dynamics in molecules, such as internal conversion, dissociation, and isomerization. These processes are of fundamental importance to a wide array of dynamics in biology, chemistry and physics. In recent years, there has been significant debate about the relative merits of strong-field ionization (SFI), which involves multi-photon absorption, versus weak-field ionization (WFI), where a single photon is absorbed, as probes of these dynamics. SFI is advantageous because it uses wavelengths that are relatively easy to generate, and one can always ionize the molecule with sufficient intensity. However, for SFI it is difficult to calculate observables, such as the time-dependent ion yield, since the calculation of the ionization dynamics including multi-photon processes is computationally expensive, and difficult to carry out for many molecular geometries. WFI has the advantage that calculations of observables are tractable. However, the generation and implementation of the appropriate wavelengths (photon energies) can be challenging, and the fixed energy of the probe can lead to technical complications in following the dynamics from excited states back down to the ground state. Here we present a quantitative comparison of the two approaches for following the excited state dynamics of two molecules, diiodomethane and uracil. The combination of internal conversion and dissociation in these molecules provides an ideal comparison of WFI and SFI as a probe. We compare the measurements with calculations of the dynamics. Our work indicates that while SFI and WFI provide qualitatively similar information about the excited state dynamics, only WFI results can be compared quantitatively with present-day calculations.

Photoinduced excited state molecular dynamics play a central role in many fundamental processes in nature. Many different approaches have been developed in order to follow these dynamics in real time. While the dream of time resolved measurements is to make "molecular movies", it is very rare that one can directly measure a molecular structure or wave function amplitude as a function of time. Rather, the most insight is typically gained by comparing experiment with theoretical calculations of observables in order to verify the calculations, and then generating the "molecular movie" from calculations. Thus, an important criterion in evaluating different measurement approaches is how easily they can be compared with theoretical calculations of the measured observable. Each time resolved experimental approach has advantages and disadvantages. For example, ultrafast electron diffraction [1–5] holds the promise of providing direct structural information as a function of time, but suffers from orientational averaging over the sample, repulsion between the electrons in a short pulse, and the group velocity mismatch between electrons and light. Ultrafast x-ray diffraction [6–9] overcomes the last two disadvantages of electron diffraction, but suffers from low scattering cross sections, and requires a large number of photons in the probe pulse - typically only available at free electron laser light sources. Optical spectroscopy approaches such as transient absorption [10–14] can provide high time resolution with a compact apparatus, but require detailed knowledge of the potential energy surfaces (electronic energies as a function of nuclear coordinates) and transition dipole moments along the reaction coordinate in order to be interpreted. Time resolved ionization spectroscopy [15–20] offers the advantage over optical spectroscopies that it is always possible to ionize, regardless of the character of the excited state. The near threshold ionization of valence electrons from excited states (for which the cross section is large) can be accomplished either in the weak field regime, with the absorption of a single ultraviolet (UV) or vacuum ultraviolet (VUV) photon ($\sim$ 6-10 eV), or in the strong field regime, with the absorption of multiple low energy near infrared photons ($\sim$ 1-3 eV) [19–25].

Here we compare weak field ionization (WFI) with strong field ionization (SFI) as probes of excited state molecular dynamics. We consider two different kinds of excited state dynamics, internal conversion and dissociation, in two different molecules, and we compare the measurements directly with high level dynamics calculations in order to assess the relative strengths and weaknesses of the two approaches. While earlier work found significant differences between multi-photon ionization with a 1.55 eV probe and single photon ionization with a 14

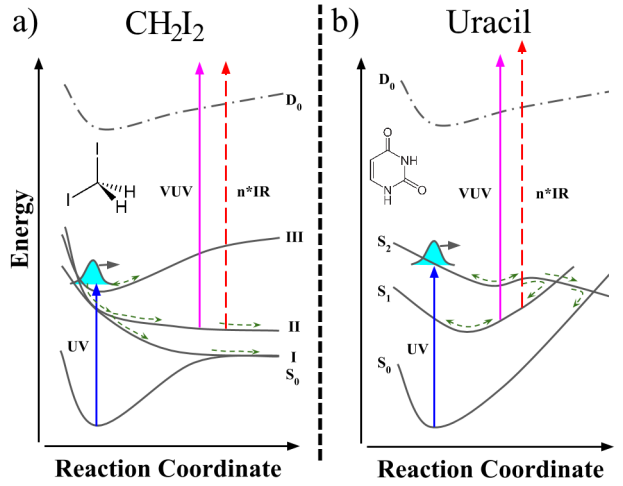


FIG. 1. Cartoons showing the excited state dynamics in a) $CH_2I_2$ after UV absorption [26], and b) uracil after UV absorption [27]. The different ionization probes for WFI (solid magenta line) and SFI (dashed red line) are also indicated.

eV probe [28], we find that WFI near threshold and SFI provide qualitatively similar results (see later), although only WFI can be compared quantitatively with calculations of the excited state dynamics. It can be shown analytically that the first-order one-photon ionization probability is directly proportional to the norm of the Dyson orbital formed by projecting the N-1 electron wave function of the final (ionic) state onto the N electron wave function of the initial (neutral) state of the molecule [29, 30]:

$$\phi^D = \sqrt{N} \int \psi_i^N(r_1, \ldots, r_N)\psi_f^{N-1}(r_2, \ldots, r_N)dr_2 \ldots dr_N, \tag{1}$$

where $\psi_i^N$ is the initial, N-electron wave function of the neutral, and $\psi_f^{N-1}$ is the final, N−1 electron wave function of the ion. The integral is over N−1 dimensions, leaving a one-electron function or orbital for $\phi^D$. The total ion yield for each molecular geometry produced by a dynamics calculation can be expressed in terms of this Dyson orbital as:

$$\text{Ion Yield} \propto \left|\left\langle \psi_k^e \left| \hat{\epsilon} \cdot \mathbf{r} \right| \phi^D \right\rangle\right|^2 \left\langle \phi^D \mid \phi^D \right\rangle, \tag{2}$$

where $\hat{\epsilon}$ is the polarization direction of the light, $\mathbf{r}$ the position operator, $\psi_k^e$ the free (continuum) electron wave function with momentum $k$, and $\left\langle \phi^D \mid \phi^D \right\rangle$ is the Dyson norm. For SFI, perturbation theory cannot be used, and there is no analog for the Dyson Norm as a good predictor of the population distribution across the ionic states. Because of this, strong field ionization requires computationally costly calculations to determine the ionization rate as a function of molecular geometry.

We carry out our comparison of WFI and SFI by following dissociation in diiodomethane, $CH_2I_2$, and internal conversion in uracil. The excited state dynamics of both diiodomethane and uracil have been the subject of intense theoretical and experimental studies [26, 27, 31–50]. Figure 1 shows one dimensional representations (cartoons) of the relevant potential energy surfaces for both molecules. In $CH_2I_2$ (panel a), earlier studies concluded that after being pumped with UV light at 260 nm, the molecule undergoes direct dissociation [49], producing $CH_2I$ and I fragments. For uracil (panel b), excitation with a pump pulse centered at 260 nm promotes the molecule to the first bright excited state, $S_2$, which is predominantly of $\pi\pi^*$ character near the ground state minimum (Franck Condon point). From $S_2$, the molecule can undergo radiationless decay via two seams of conical intersections $S_2/S_1$ and $S_1/S_0$. It is generally accepted that there is population trapping on $S_1$, while the extent of trapping on $S_2$ depends on the barrier on that surface. A cartoon illustrating uracil's relaxation dynamics can be seen in Fig. 1 b). While intersystem crossing has been found to play a role in the relaxation dynamics of uracil [43], triplet states are not shown in the cartoon for the sake of simplicity.

In conjunction with a time-of-flight mass spectrometer (TOFMS), we make use of ultrafast UV (260 nm, 4.8 eV) and Vacuum-UV (VUV) pulses (156 nm, 7.95 eV) to perform pump-probe ion yield measurements. The ultrafast UV and VUV pulses are generated from a Ti:Sapphire laser system (1.3 mJ, 1 kHz, 30 fs, 780 nm, 1.55 eV). The impulse response function (IRF) of our experimental apparatus, limited largely by our pump and probe pulse durations, is characterized by preforming VUV-pump UV-probe experiments on ethylene. Ethylene undergoes rapid internal conversion after being pumped in the VUV [51, 52], hence it can be used to extract the IRF of our system. The IRF for our apparatus is about 100 fs, although the uracil measurements were carried out before the most recent upgrade and had an IRF of about 200 fs. Gas-phase diiodomethane is injected as an effusive molecular beam at 25°C. Gas-phase uracil molecules are injected into the vacuum chamber as an effusive molecular beam with an oven at 200°C. More details about the experimental setup and a schematic of the system can be found in [53].

For WFI UV-VUV pump-probe measurements performed on diiodomethane, $CH_2I_2$, we observed transient ion yields for the parent ion, $CH_2I_2^+$, and the fragment ion, $CH_2I^+$. The total energy available following the absorption of one photon from each of the pump and probe pulses is 12.75 eV. The observation of the parent and this fragment ion are consistent with previous measurements [54–57], where the appearance energies (AE) of $CH_2I_2^+$ and $CH_2I^+$ are about 9.46 and 10.49 eV respectively.

The total ion yield pump-probe signal for $CH_2I_2$ both SFI and WFI can be seen in Fig. 2 a) plotted on the same graph. Negative time delays are shaded gray, because we want to focus our attention on positive time delays where the UV-pump precedes the VUV-probe. Both methods

reveal a very fast ∼ 50 fs decay, but the SFI measurements show a longer component to the decay (∼ 500 fs). Since the excited state dynamics in both experiments are identical, the differences in the measured signals must be due to differences in the interaction between the molecules and the probe pulse - i.e. the difference in the measurements comes from the different sensitivities that WFI and SFI have to the excited state dynamics. We believe that this longer decay in the SFI $CH_2I_2$ pump-probe signal is due to a multiphoton resonance which enhances the ion yield as the molecule dissociates [19–25, 28]. As the wavepacket dissociates on the neutral excited state, the molecular structure can be such that n-photons ($n < IP/h\nu$) from the strong field probe can come into resonance with an intermediate state, between the excited state and the continuum, increasing the ionization rate. This interpretation is consistent with earlier measurements of multi-photon resonances in strong field ionization of halogenated methane molecules [20]. Since one doesn't know *a priori* (i.e. without carrying out detailed electronic structure calculations for different molecular geometries) whether resonances will modify the ion signal versus structure/configuration for SFI, one cannot know whether the SFI signal versus time is directly connected to changes in molecular geometry, or distorted by the intermediate dynamic resonances that occur.

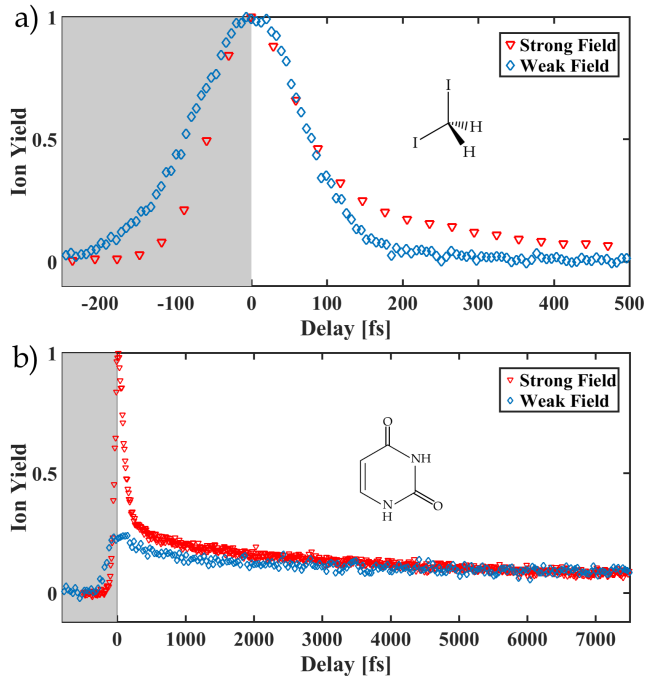


FIG. 2. a) Weak-field UV-VUV and strong-field UV-IR total ion yield pump-probe measurement on diiodomethane. b) Weak-field UV-VUV and strong-field UV-IR total ion yield pump-probe measurement on uracil.

In the uracil UV-VUV WFI pump-probe experiments, we measured the parent ion, $C_4H_4N_2O_2^+$, and the fragment ion with mass 69 in atomic mass units (AMU) in the TOFMS. These observations are consistent with photon impact AE (9.15 ± 0.03 eV for the parent ion and 10.95 ± 0.05 eV for the fragment ion, $C_3H_3NO^+$ (mass 69 AMU) [58]). The appearance energies of other fragments are all greater than 12.75 eV.

The total ion pump-probe signal for WFI UV-VUV pump-probe experiments and SFI UV-IR pump-probe experiments on uracil can be seen in Fig. 2 b). For SFI, we find that the exact structure of the pump-probe signal can vary with the intensity of the probe, which highlights one of the major difficulties with working with the SFI as a probing mechanism (a more detailed discussion of this can be found in Appendix I: Error Bar Determination for Uracil Strong-Field Ionization Measurements).

Analyzing the WFI and SFI results on uracil and performing $\chi^2$ fitting, it became clear that the pump-probe signals consist of two decay timescales, one short and one long (details of this fitting can be seen in Appendix I: $CH_2I_2$ and Uracil Fitting Results). The SFI and WFI signals have similar long decay timescales, but they differ significantly for the shorter time-scales. The SFI yield has a much sharper peak at zero time delay than the WFI yield. As in the case of $CH_2I_2$, given the same dynamics excited by the pump-pulse, the difference in signal must derive from differences in the sensitivity of the two probes. The sharp peak near zero delay in the SFI data could be due to multiple effects: an enhancement in the multi-photon ionization yield due to the overlap of the pump and probe pulses, a distortion of the potential energy surfaces by the strong field of the probe pulse, or to the greater sensitivity of the SFI yield to wave packet motion away from the FC region. In any case, it is clear that SFI exaggerates, or distorts the motion of the wave packet near the FC region.

Figure 2 illustrates one of the difficulties in only looking at decay constants to compare an experiment to theory. The SFI measurements can not be fit to a single exponential decay in either of the two cases we consider here. Comparing one decay time from a multi-parameter fit with several decay components to theory can be very misleading because the fit parameters can be coupled and the relative importance of a given decay time can depend sensitively on the details of the fitting procedure. As a result, we argue that the best test of quantitative agreement between a particular theory and experiment is to plot the experiment and theory together on the same graph.

The differences between WFI and SFI as a probe of excited state dynamics are highlighted by comparing theory and experiment. For both molecules, we carried out trajectory surface hopping calculations of the dynamics, using the SHARC [59–61] and NEWTON-X [62, 63] packages. The ionization yield as a function of delay was

based upon the excited state populations as a function of time, with Dyson norms calculated in addition for the case of $CH_2I_2$.

For $CH_2I_2$ the calculations were done with SHARC based on MS-CASPT2 (multi-state complete active space perturbation theory second order) level of theory [64] and coupled with Dyson norm calculations [65] in order to carry out a thorough comparison to the experimental results. The convolution of the calculations with the IRF of our apparatus, acquired from the ethylene VUV-UV pump-probe scans, is required to accurately compare the experimental results to the theory (further details in Appendix II: $CH_2I_2$ Calculation Details). The results of this analysis can be seen in Fig. 3 a).

For uracil, CASPT2 analytic gradients are not available and numerical gradients would be computationally prohibitive. Therefore, dynamics were carried out on potentials calculated at the complete active space self consistent field (CASSCF) and multireference configuration interaction with single excitations (MRCIS) levels of theory using the Columbus 7.0 and NewtonX packages [66–68]. CASSCF dynamics calculations were performed to track the dynamics for 1 ps, and MRCIS dynamics calculations, due to the greater computational complexity, were carried out for only 500 fs. MRCIS is a higher level of theory than CASSCF, and is used to check the validity of the CASSCF calculations. To compare these results to the UV-VUV pump-probe signal we look at the total ion yield and assume that the total excited state populations ($S_1$ and $S_2$) are ionized, taking the $S_1$ and $S_2$ populations as the total ion signal. Dyson norms are not used for the uracil calculations, because they don't appear to have significant variation for different geometries along $S_1$ and $S_2$. In earlier work we studied the variation in the Dyson norms for ionization of uracil from $S_1$ and $S_2$ [27]. Our calculations indicated that there were no dramatic differences in the Dyson norms on these states in moving between the $S_2$ minimum, the $S_1$ minimum, and the $S_1/S_2$ CI geometries. Since only these two states are involved in the dynamics and there is not much variation in the Dyson norms from these two states, we did not calculate them at each point in the trajectories. Again, the results of the computation were convolved with the IRF of the system for an accurate comparison to the experiment. The results of this analysis can be seen in Fig. 3 b). The agreement between the experimental WFI data and the MRCIS and CASSCF calculations is quite good (details of the uracil calculations can be found in Appendix II: Uracil Calculation Details). A more detailed analysis of the excited state dynamics calculations for both uracil and $CH_2I_2$ is the subject of forthcoming papers.

The agreement between the WFI experimental data and the calculations highlights a key difference between SFI and WFI. Even though SFI and WFI are both able to provide a qualitative picture of the relaxation dynamics, there are still quantitative differences for both molecules.

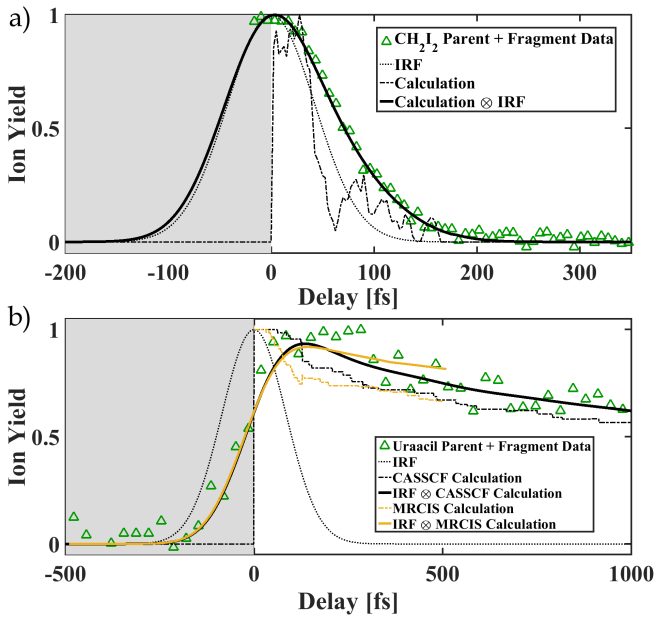


FIG. 3. a) $CH_2I_2$ WFI UV-VUV pump-probe total ion yield data (green triangle), CASPT2 dynamics with Dyson norms calculation on $CH_2I_2$ (dotted-dashed line), IRF of our apparatus (dotted line), and convolution of the calculation and the IRF of the system (solid line). b) Uracil WFI UV-VUV pump-probe total ion yield data (upward facing green triangle), CASSCF calculation for uracil (black dotted-dashed line), impulse response function (IRF) of our apparatus (black dotted line), convolution of the CASSCF calculation and the IRF of the system (solid black line), MRCIS calculation for uracil (gold dotted-dashed line), and convolution of the MRCIS calculation and the IRF of the system (solid gold line).

By qualitative agreement, we mean that the decay curves look similar (i.e. exponential or multiexponential behavior), yield timescales of the same order of magnitude, and show similar trends (i.e. the ionization yield for Uracil has a long tail for both SFI and WFI whereas the WFI and SFI ion yields for $CH_2I_2$ do not). However, in order to test the validity of a calculation or discriminate between two different theories, quantitative agreement is required. We argue that the best test of quantitative agreement is to plot experimental and theoretical results together on the same graph. A direct comparison between SFI measurements and calculations of the excited state dynamics is impossible without explicit calculations of the SFI dynamics, which are computationally expensive and unfeasible for the timescales involved in the excited state dynamics probed here. The qualitative agreement between WFI and SFI measurements of the excited state dynamics illustrates the fact that both ion yields contain similar information on the excited state dynamics. The quantitative agreement between the WFI measurements and calculations, however, allows one to interpret and understand the dynamics at a level of detail not possible with SFI.

We gratefully acknowledge support from the Department of Energy under awards number DEFG02-08ER15983 and DEFG02-08ER15984. This project was partly supported by the Government of Hungary and the European Regional Development Fund under grant VEKOP-2.3.2-16-2017-00015. The computational results presented have been achieved in part using the Vienna Scientific Cluster (VSC). Part of the computational work used the Extreme Science and Engineering Discovery Environment (XSEDE), which is supported by National Science Foundation grant number ACI-1548562.

[1] J. C. Williamson, J. Cao, H. Ihee, H. Frey, and A. H. Zewail, Nature **386**, 159 (1997).
[2] M. Dantus, S. B. Kim, J. C. Williamson, and A. H. Zewail, The Journal of Physical Chemistry **98**, 2782 (1994).
[3] P. Reckenthaeler, M. Centurion, W. Fuß, S. A. Trushin, F. Krausz, and E. E. Fill, Physical Review Letters **102**, 213001 (2009).
[4] S. Weathersby, G. Brown, M. Centurion, T. Chase, R. Coffee, J. Corbett, J. Eichner, J. Frisch, A. Fry, M. Gühr, et al., Review of Scientific Instruments **86**, 073702 (2015).
[5] J. Yang, M. Guehr, X. Shen, R. Li, T. Vecchione, R. Coffee, J. Corbett, A. Fry, N. Hartmann, C. Hast, et al., Physical Review Letters **117**, 153002 (2016).
[6] J. Cao and K. R. Wilson, The Journal of Physical Chemistry A **102**, 9523 (1998).
[7] K. Gaffney and H. Chapman, Science **316**, 1444 (2007).
[8] F. Schotte, M. Lim, T. A. Jackson, A. V. Smirnov, J. Soman, J. S. Olson, G. N. Phillips, M. Wulff, and P. A. Anfinrud, Science **300**, 1944 (2003).
[9] M. P. Minitti, J. M. Budarz, A. Kirrander, J. S. Robinson, D. Ratner, T. J. Lane, D. Zhu, J. M. Glownia, M. Kozina, H. T. Lemke, et al., Phys. Rev. Lett. **114**, 255501 (2015).
[10] R. Berera, R. van Grondelle, and J. T. Kennis, Photosynthesis Research **101**, 105 (2009).
[11] C. Ruckebusch, M. Sliwa, P. d. Pernot, A. De Juan, and R. Tauler, Journal of Photochemistry and Photobiology C: Photochemistry Reviews **13**, 1 (2012).
[12] C. Wan, T. Fiebig, S. O. Kelley, C. R. Treadway, J. K. Barton, and A. H. Zewail, Proceedings of the National Academy of Sciences **96**, 6014 (1999).
[13] J.-M. L. Pecourt, J. Peon, and B. Kohler, Journal of the American Chemical Society **122**, 9348 (2000).
[14] W. J. Schreier, T. E. Schrader, F. O. Koller, P. Gilch, C. E. Crespo-Hernández, V. N. Swaminathan, T. Carell, W. Zinth, and B. Kohler, Science **315**, 625 (2007).
[15] A. Stolow and J. G. Underwood, arXiv preprint arXiv:1507.02204 (2015).
[16] A. Stolow, A. E. Bragg, and D. M. Neumark, Chemical ROeviews **104**, 1719 (2004).
[17] V. Blanchet, M. Z. Zgierski, T. Seideman, and A. Stolow, Nature **401**, 52 (1999).
[18] S. Ullrich, T. Schultz, M. Z. Zgierski, and A. Stolow, Physical Chemistry Chemical Physics **6**, 2796 (2004).
[19] P. Sándor, V. Tagliamonti, A. Zhao, T. Rozgonyi, M. Ruckenbauer, P. Marquetand, and T. Weinacht, Physical Review Letters **116**, 063002 (2016).
[20] V. Tagliamonti, P. Sándor, A. Zhao, T. Rozgonyi, P. Marquetand, and T. Weinacht, Physical Review A **93**, 051401 (2016).
[21] I. Wilkinson, A. E. Boguslavskiy, J. Mikosch, J. B. Bertrand, H. J. Wörner, D. M. Villeneuve, M. Spanner, S. Patchkovskii, and A. Stolow, The Journal of Chemical Physics **140**, 204301 (2014).
[22] C. Okabe, T. Nakabayashi, Y. Inokuchi, N. Nishi, and H. Sekiya, The Journal of Chemical Physics **121**, 9436 (2004).
[23] S. Trushin, W. Fuss, and W. Schmid, Chemical Physics **259**, 313 (2000).
[24] S. Trushin, W. Fuss, W. Schmid, and K. Kompa, The Journal of Physical Chemistry A **102**, 4129 (1998).
[25] V. Tagliamonti, B. Kaufman, A. Zhao, T. Rozgonyi, P. Marquetand, and T. Weinacht, Physical Review A **96**, 021401 (2017).
[26] B. W. Toulson, J. P. Alaniz, J. G. Hill, and C. Murray, Physical Chemistry Chemical Physics **18**, 11091 (2016).
[27] S. Matsika, M. Spanner, M. Kotur, and T. C. Weinacht, The Journal of Physical Chemistry A **117**, 12796 (2013).
[28] M. Koch, T. J. Wolf, and M. Gühr, Physical Review A **91**, 031403 (2015).
[29] M. Spanner, S. Patchkovskii, C. Zhou, S. Matsika, M. Kotur, and T. C. Weinacht, Physical Review A **86**, 053406 (2012).
[30] C. Melania Oana and A. I. Krylov, The Journal of Chemical Physics **127**, 234106 (2007).
[31] H. Kang, K. T. Lee, B. Jung, Y. J. Ko, and S. K. Kim, Journal of the American Chemical Society **124**, 12958 (2002).
[32] S. Ullrich, T. Schultz, M. Z. Zgierski, and A. Stolow, Physical Chemistry Chemical Physics **6**, 2796 (2004).
[33] C. Canuel, M. Mons, F. Piuzzi, B. Tardivel, I. Dimicoli, and M. Elhanine, The Journal of Chemical Physics **122**, 074316 (2005).
[34] T. Gustavsson, Á. Bányász, E. Lazzarotto, D. Markovitsi, G. Scalmani, M. J. Frisch, V. Barone, and R. Improta, Journal of the American Chemical Society **128**, 607 (2006).
[35] T. Gustavsson, N. Sarkar, E. Lazzarotto, D. Markovitsi, and R. Improta, Chemical Physics Letters **429**, 551 (2006).
[36] H. R. Hudock, B. G. Levine, A. L. Thompson, H. Satzger, D. Townsend, N. Gador, S. Ullrich, A. Stolow, and T. J. Martinez, The Journal of Physical Chemistry A **111**, 8500 (2007).
[37] M. K. Shukla and J. Leszczynski, in *Radiation Induced Molecular Phenomena in Nucleic Acids* (Springer, 2008), pp. 265–299.
[38] Z. Lan, E. Fabiano, and W. Thiel, The Journal of Physical Chemistry B **113**, 3548 (2009).
[39] M. Barbatti, A. J. Aquino, J. J. Szymczak, D. Nachtigallová, P. Hobza, and H. Lischka, Proceedings of the National Academy of Sciences **107**, 21453 (2010).
[40] D. Nachtigallová, A. J. Aquino, J. J. Szymczak, M. Barbatti, P. Hobza, and H. Lischka, The Journal of Physical Chemistry A **115**, 5247 (2011).
[41] M. Kotur, T. C. Weinacht, C. Zhou, and S. Matsika, IEEE Journal of Selected Topics in Quantum Electronics **18**, 187 (2012).
[42] B. P. Fingerhut, K. E. Dorfman, and S. Mukamel, The

Journal of Physical Chemistry Letters **4**, 1933 (2013).
[43] M. Richter, S. Mai, P. Marquetand, and L. González, Physical Chemistry Chemical Physics **16**, 24423 (2014).
[44] M. Kawasaki, S. Lee, and R. Bersohn, The Journal of Chemical Physics **63**, 809 (1975).
[45] J. Zhang, E. J. Heller, D. Huber, D. G. Imre, and D. Tannor, The Journal of Chemical Physics **89**, 3602 (1988).
[46] X. Zheng and D. L. Phillips, Chemical Physics Letters **324**, 175 (2000).
[47] S. Roszak, W. Koski, J. Kaufman, and K. Balasubramanian, SAR and QSAR in Environmental Research **11**, 383 (2001).
[48] M. Odelius, M. Kadi, J. Davidsson, and A. N. Tarnovsky, The Journal of Chemical Physics **121**, 2208 (2004).
[49] Y.-J. Liu, L. De Vico, R. Lindh, and W.-H. Fang, ChemPhysChem **8**, 890 (2007).
[50] A. Mandal, P. J. Singh, A. Shastri, and B. Jagatap, The Journal of Chemical Physics **140**, 194312 (2014).
[51] P. Farmanara, O. Steinkellner, M. Wick, M. Wittmann, G. Korn, V. Stert, and W. Radloff, The Journal of Chemical Physics **111**, 6264 (1999).
[52] T. Allison, Ph.D. thesis, UC Berkeley: Physics (2010).
[53] S. L. Horton, Y. Liu, P. Chakraborty, S. Matsika, and T. Weinacht, The Journal of Chemical Physics **146**, 064306 (2017).
[54] J. L. Holmes, F. Lossing, and R. McFarlane, International Journal of Mass Spectrometry and Ion Processes **86**, 209 (1988).
[55] B. P. Tsal, T. Baer, A. S. Werner, and S. F. Lin, The Journal of Physical Chemistry **79**, 570 (1975).
[56] W. von Niessen, L. Åsbrink, and G. Bieri, Journal of Electron Spectroscopy and Related Phenomena **26**, 173 (1982).
[57] A. Potts, H. Lempka, D. Streets, and W. Price, Philosophical Transactions for the Royal Society of London. Series A, Mathematical and Physical Sciences pp. 59–76 (1970).
[58] H.-W. Jochims, M. Schwell, H. Baumgärtel, and S. Leach, Chemical Physics **314**, 263 (2005).
[59] S. Mai, M. Richter, M. Heindl, M. F. S. J. Menger, A. Atkins, M. Ruckenbauer, F. Plasser, M. Oppel, P. Marquetand, and L. González, *Sharc2.0: Surface hopping including arbitrary couplings program package for non-adiabatic dynamics*, sharc-md.org (2018).
[60] M. Richter, P. Marquetand, J. González-Vázquez, I. Sola, and L. González, J. Chem. Theory Comput. **7**, 1253 (2011).
[61] S. Mai, P. Marquetand, and L. González, Wiley Interdisciplinary Reviews: Computational Molecular Science p. e1370 (2018).
[62] M. Barbatti, M. Ruckenbauer, F. Plasser, J. Pittner, G. Granucci, M. Persico, and H. Lischka, Wiley Interdisciplinary Reviews: Computational Molecular Science **4**, 26 (2014).
[63] M. Barbatti, G. Granucci, M. Ruckenbauer, F. Plasser, R. Crespo-Otero, J. Pittner, M. Persico, and H. Lischka, *Newton-x: A package for newtonian dynamics close to the crossing seam, version 2*, www.newtonx.org (2016).
[64] S. Mai, P. Marquetand, and L. González, The Journal of Physical Chemistry Letters **7**, 1978 (2016).
[65] M. Ruckenbauer, S. Mai, P. Marquetand, and L. González, Scientific Reports **6**, 35522 (2016).
[66] H. Lischka, T. Müller, P. G. Szalay, I. Shavitt, R. M. Pitzer, and R. Shepard, Wiley Interdisciplinary Reviews: Computational Molecular Science **1**, 191 (2011).
[67] H. Lischka, R. Shepard, R. M. Pitzer, I. Shavitt, M. Dallos, T. Müller, P. G. Szalay, M. Seth, G. S. Kedziora, S. Yabushita, et al., Physical Chemistry Chemical Physics **3**, 664 (2001).
[68] H. Lischka, R. Shepard, I. Shavitt, R. Pitzer, M. Dallos, T. Müller, P. Szalay, F. Brown, R. Ahlrichs, H. Böhm, et al., *Columbus, an ab initio electronic structure program* (2012).
[69] F. Aquilante, J. Autschbach, R. K. Carlson, L. F. Chibotaru, M. G. Delcey, L. De Vico, N. Ferré, L. M. Frutos, L. Gagliardi, M. Garavelli, et al., Journal of computational chemistry **37**, 506 (2016).
[70] J. P. Zobel, J. J. Nogueira, and L. González, Chemical science **8**, 1482 (2017).
[71] N. Forsberg and P.-Å. Malmqvist, Chemical Physics Letters **274**, 196 (1997).
[72] M. Reiher, Rev. Comput. Mol. Sci **2**, 139 (2012).
[73] P. Å. Malmqvist, B. O. Roos, and B. Schimmelpfennig, Chemical physics letters **357**, 230 (2002).
[74] B. Schimmelpfennig, Stockholm University (1996).
[75] G. Granucci, M. Persico, and A. Toniolo, The Journal of Chemical Physics **114**, 10608 (2001).
[76] G. Granucci and M. Persico, The Journal of chemical physics **126**, 134114 (2007).
[77] M. Barbatti, G. Granucci, M. Persico, M. Ruckenbauer, M. Vazdar, M. Eckert-Maksić, and H. Lischka, Journal of Photochemistry and Photobiology A: Chemistry **190**, 228 (2007).
[78] M. Ruckenbauer, S. Mai, P. Marquetand, and L. González, Scientific Reports **6**, 35522 (2016).
[79] F. Plasser, M. Ruckenbauer, S. Mai, M. Oppel, P. Marquetand, and L. González, Journal of chemical theory and computation **12**, 1207 (2016).
[80] R. A. Gaussian09, Inc., Wallingford CT (2009).
[81] C. Zhu, A. W. Jasper, and D. G. Truhlar, Journal of chemical theory and computation **1**, 527 (2005).
[82] J. Towns, T. Cockerill, M. Dahan, I. Foster, K. Gaither, A. Grimshaw, V. Hazlewood, S. Lathrop, D. Lifka, G. D. Peterson, et al., Computing in Science & Engineering **16**, 62 (2014).
[83] V. Mozhayskiy and A. Krylov, Available at iopenshell. usc. edu/downloads/ezspectrum/r (2014).
[84] Y. Shao, Z. Gan, E. Epifanovsky, A. Gilbert, M. Wormit, J. Kussmann, A. Lange, A. Behn, J. Deng, X. Feng, et al., Molecular Physics **113**, 184 (2015).

## APPENDIX I: FITTING DETAILS

### Fitting Function Details

The dichroic mirror which combines the UV pump pulse and VUV probe pulse does not act as a perfect filter for the residual UV used to generate the VUV, and a fraction (between $5-10\%$) of this UV is reflected and generates a UV-UV pump-probe background signal in the uracil data. The UV-UV pump-probe signal has to be filtered out from the UV-VUV pump-probe signal (the details into separating the two signals can be seen in the next section). The fitting function for the uracil weak-

field data is:

$$f(t) = e^{-\frac{(t-t_0)^2}{2\sigma^2}} \otimes \left[\Theta(t-t_0)\left(A_1 e^{-\frac{(t-t_0)}{\tau_1}} + A_2 e^{-\frac{(t-t_0)}{\tau_2}} + A_3\right)\right] + e^{-\frac{(t-t_0')^2}{2\sigma'^2}} \otimes \left[\Theta(t-t_0')\left(A' e^{-\frac{(t-t_0')}{\tau'}}\right)\right]. \quad (3)$$

This fitting function for the weak-field data has two main components: the first component is the UV-VUV pump-probe signal, and the second is the UV-UV pump-probe signal. We assume that our UV and VUV pulses are Gaussian in time, so that our apparatus' impulse response time, $\sigma$, is dictated by our pulse durations. Therefore, $\sigma$ is essentially the convolution of our pump and probe pulse durations. $t_0$ corresponds to time-zero (where the UV and VUV pulses are overlapped). $t_0'$ represents the time-zero for the two UV-pulses -i.e. where the two UV-pulses are overlapped, and $\sigma'$ is the time resolution of the UV-UV signal in our apparatus. $\sigma'$ is essentially the convolution of the two UV pulse durations. $A'$ and $\tau'$ are the amplitude and decay constant for the molecular decay. $\Theta$ is the Heaviside step function, and is used to ensure that the molecular dynamics cannot initiate until the excited state is populated.

The UV-VUV fit also consists of two exponential decays and a constant. $A_1$ and $\tau_1$ characterize the amplitude and decay constant for the first decay. $A_2$ and $\tau_2$ are the amplitude and decay constant of the second decay. The constant, $A_3$, represents the population that has a decay constant on the order of nanoseconds, so on our timescales it manifests itself as a constant.

In the weak-field data there is a plateau in both the parent and the fragment ion data. By a plateau we mean that the ion yield from before time-zero is lower than the ion yield at long time delays (if the molecule were relaxing back to its ground state we would expect these levels to be equal on either side of time-zero). As mentioned before, this plateau is encapsulated in the fit as $A_3$. Longer delay scans of 20 ps were taken for uracil and it was found that after 7 ps the ion yield shows no more significant decay and that the yield reaches a plateau.

The fitting function for the weak-field $CH_2I_2$ data and for the strong-field $CH_2I_2$ parent ion data is:

$$f(t) = e^{-\frac{(t-t_0)^2}{2\sigma^2}} \otimes \left[\Theta(t-t_0)\left(A_1 e^{-\frac{(t-t_0)}{\tau_1}}\right)\right]. \quad (4)$$

The fitting function for the strong-field $CH_2I_2$ fragments ion data is:

$$f(t) = e^{-\frac{(t-t_0)^2}{2\sigma^2}} \otimes \left[\Theta(t-t_0)\left(A_1 e^{-\frac{(t-t_0)}{\tau_1}} + A_2 e^{-\frac{(t-t_0)}{\tau_2}}\right)\right]. \quad (5)$$

### UV-UV Pump-Probe Peak Subtraction

After the VUV is generated in an argon gas cell the VUV-pulse passes through a 500 $\mu$m thick $CaF_2$ window into an interaction chamber, which is maintained at a pressure of $10^{-7}$ Torr. The VUV-pulse first passes under the repeller plates of our TOFMS. It is then reflected by a dichroic mirror of radius of curvature $R = 268$ mm. The mirror has a high reflectivity coating of $> 90\%$ at $0°$ for $156 - 160$ nm light and $< 10\%$ reflectivity for 260 nm and 800 nm. This enables the residual UV and IR radiation left over from VUV generation to be separated from the VUV.

While less than 10% of the UV is reflected by the dichroic mirror, it is enough UV to also generate multiphoton absorption, and leads to a UV pump UV probe signal. The group velocity difference between the UV and VUV passing through the 500 $\mu$m thick $CaF_2$ window leads to a 1 ps delay between the VUV and the UV pulses reflected by the dichroic mirror. UV-UV background scans are taken to subtract the UV-UV signal from the UV-VUV signal.

In order to properly look at the UV-VUV pump-probe dynamics, the UV-UV pump-probe signal must be separated from the UV-VUV pump-probe signal. In Fig. 4 the green diamonds represent the raw uracil parent ion yield. It is evident that there are two peaks. The first peak, at 0 fs, is the UV-VUV pump-probe signal, and the second peak, at $\sim 1000$ fs, is the UV-UV pump-probe signal.

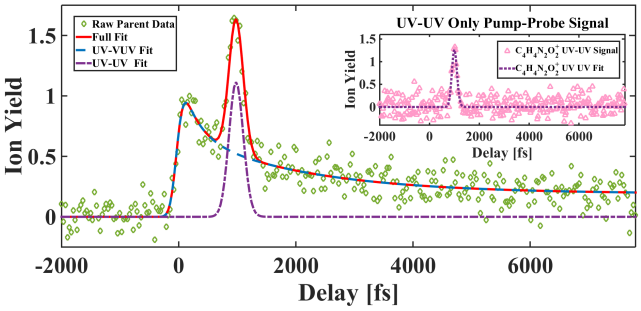


FIG. 4. The green diamonds are the raw data collected for the parent ion that contain both the UV-VUV and UV-UV pump-probe signals. The red solid curve is the full fit given by Eq. 1. The dashed cyan curve is the UV-VUV fit component. The purple dashed-dotted curve is the UV-UV fit component. The inset plot is contains UV-UV pump-probe data taken without any VUV present. The light blue diamonds are the UV-UV pump-probe data and the dashed-dotted purple line is the fit to the UV-UV data.

Background pump-probe scans were performed with only the UV in the chamber in order to characterize the background signal, which can be seen in the inset of Fig. 4. From these background scans it is possible to extract $t_0'$, $\sigma'$, and $\tau'$ to use in Eq. 1, which are then fixed when

doing the fitting of the combined UV-VUV and UV-UV pump-probe scan.

In Fig. 4, the red curve is the complete fit, shown in Eq. 1, with both the UV-VUV and UV-UV pump-probe components. The purple dashed-dotted curve in the main plot of Fig. 4 is the fit to the UV-UV pump-probe component, and is the same as the purple dashed-dotted line in the inset (except for the amplitude factor $A'$). The cyan dashed curve is the UV-VUV pump-probe fit. Characterizing the UV-UV background signal independently of the VUV-signal enables fitting to the UV-UV pump-probe data, and then it is possible to subtract the UV-UV contribution from the raw data and generate the plots in Fig. 2 a) in the main text.

No UV-UV pump-probe peak subtraction is needed for the weak-field $CH_2I_2$ data, because the molecular dynamics are very fast and the dynamics are completed before the UV-UV pulse comes with a 1ps delay.

### $CH_2I_2$ and Uracil Fitting Results

WFI UV-VUV pump-probe scans for the parent and the fragment ions together with fits can be seen in Fig. 5 a). The SFI results and fitting of $CH_2I_2$ can be seen in Fig. 5 b). $\chi^2$-fitting is performed to determine the decay constants. Each pump-probe scan is fit to an exponential or a sum of two exponentials convolved with the IRF of our apparatus (Gaussian). The minimum number of exponentials are used that give a fit where $\chi^2_\nu \sim 1$.

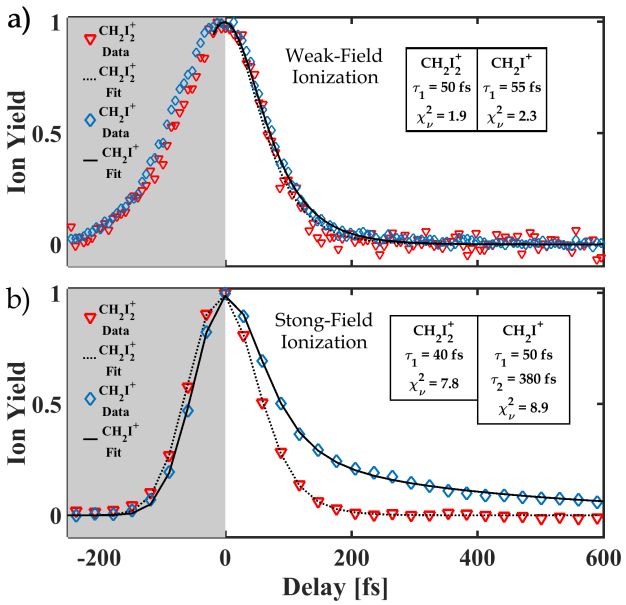


FIG. 5. a) Weak-field UV-VUV pump-probe measurement and fitting on diiodomethane. b) Strong-field UV-IR pump-probe measurement and fitting on diiodomethane.

The results of the fitting of the parent ion for both SFI and WFI give consistent decay constants, but some discrepancy between the yields for the two methods appears in the fragment ion data. Both methods reveal a very fast $\sim$ 50 fs decay, but the SFI data also show a longer component to the decay with $\tau = 380$ fs.

The parent and fragment ion yields along with fits for WFI UV-VUV pump-probe experiments on uracil can be seen in Fig. 6 a). In uracil, error bars for a fit parameter in the WFI scans are determined by the range over which $\chi^2$ changes by 1 from its minimum value. For SFI, we found that the variation in decay times for different pump probe scans was larger than the uncertainty determined from a given fit. Therefore, the error bars were determined by performing the measurement multiple times and refitting the data, with the standard deviation from the mean for the multiple measurements taken as the error bar. A more detailed discussion of the data and error analysis can be found in Appendix I: .

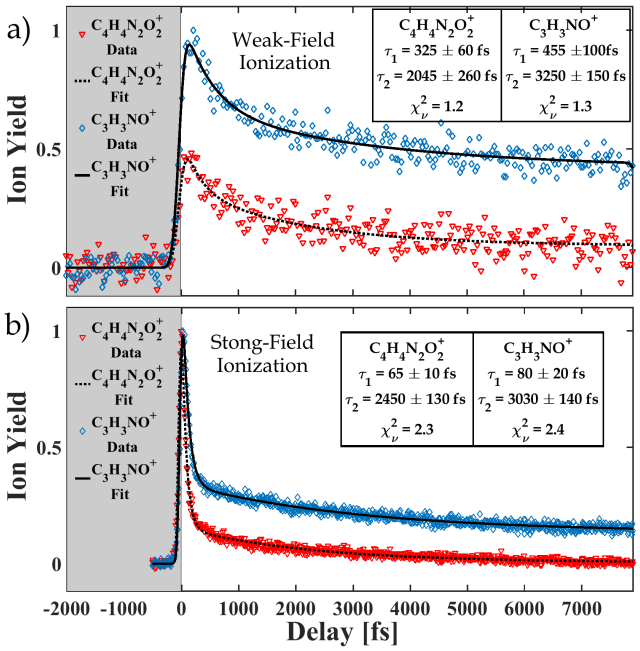


FIG. 6. a) Weak-field UV-VUV pump-probe experiment on uracil. b) Strong-field UV-IR pump-probe experiment on uracil

For the parent ion, $C_4H_4N_2O_2^+$, the shorter decay, $\tau_1 = 325 \pm 50$ fs, is consistent with either a rapid motion away from the Frank-Condon region, or a portion of the wavepacket making a rapid non-adiabatic transition to $S_1$ or $S_0$. The longer decay constant, $\tau_2 = 2045 \pm 260$ fs, suggests that a portion of the wavepacket is trapped in a minimum for several picoseconds. For the fragment ion, $C_3H_3NO^+$, time constants of $\tau_1 = 455 \pm 100$ fs and $\tau_2 = 3250 \pm 150$ fs were extracted. The SFI results and fitting can be seen in Fig. 6 b). For the parent ion $\tau_1 = 65 \pm 10$ fs and $\tau_2 = 2450 \pm 130$ fs. For the fragment ion $\tau_1 = 80 \pm 20$ fs and $\tau_2 = 3030 \pm 140$ fs.

### Error Bar determination for Uracil Strong-Field Ionization Measurements

The strong field ionization results for uracil are sensitive to systematic effects (such as the laser intensity of the strong field probe), and these systematic effects appear to be the main source of error in the fitting for these experiments. To account for these in the calculation of uncertainties in the strong-field uracil data, four different data sets with varying probe intensity were analyzed. Each data set was individually fitted. The results of this fitting can be seen in Fig. 7 for both the parent and the fragment ion decay constants. The mean, $\mu$, and the mean plus and minus the standard deviation, $\sigma$, are also plotted. Unlike in the weak-field experiments, the error extracted from the individual data sets from $\Delta\chi^2 = 1$ is much smaller than the variation in the decay constants from data set to data set. This indicates that the dominant source of error in these experiments is systematic.

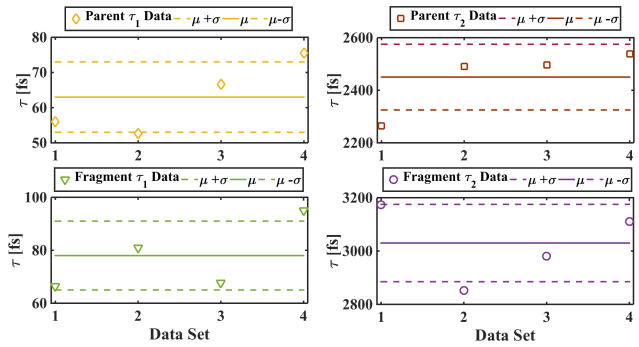


FIG. 7. Uracil decay constants extracted from strong field ionization experiments with varying probe intensities in order to determine the systematic errors in the experiment, so error bars can be set on our decay constants.

### Time Resolution Check for Comparison of $CH_2I_2$ Calculations to the Experimental Data

In order to compare the CASPT2 dynamics and Dyson norm calculation on diiodomethane with the experimental data, we had to convolve the calculation with the temporal response of our system (which is 100 fs). As a test of whether this convolution obscures the underlying molecular dynamics, we compare the experimental measurements with calculations where we stretched or contracted the dynamics by factors of 1.5 and 2 prior to the convolution. We plot the stretched and contracted calculations together with the data in Fig. 8. It is clear from the figure that the measurements agree well with the original calculation data, while disagreeing with the stretched or contracted data. This indicates that the measurement contains more information than just an upper bound on the dynamics or timescale.

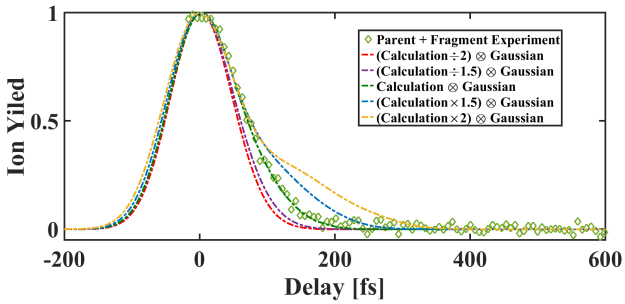


FIG. 8. Scaling the CASPT2 dynamics and Dyson norm calculation on diiodomethane and convolving with a 100 fs FWHM Gaussian to check the comparison between theory and experiment.

## APPENDIX II: CALCULATION DETAILS

### $CH_2I_2$ Calculation Details

In order to carry out the excited-stated dynamics simulations for $CH_2I_2$, we used SHARC (Surface Hopping including ARbitrary Couplings) [59–61] interfaced with Molcas 8.0 [69]. The electronic structure calculations of the neutral molecule were performed with MS-CASPT2(12,8)/ano-rcc-vdzp (multi-state complete active space perturbation theory second order) based on SA(5/4)-CASSCF(12,8) (complete active space self-consistent field with 12 electrons in 8 orbitals and state-averaging including either 5 singlet or 4 triplet states) calculations. The IPEA shift was set to zero, as this was found to improve the results in combination with the small double-$\zeta$ basis set [70]. However, to avoid intruder states and ensure a stable propagation in the dynamics simulations, an imaginary shift of 0.3 Hartree was added [71]. In order to account for scalar-relativistic effects, the second-order Douglas-Kroll-Hess (DKH) Hamiltonian [72] was employed while spin-orbit couplings (SOCs) were computed with the RASSI [73] and AMFI [74] formalisms. The dynamics were run employing the velocity-Verlet algorithm with a time step of 0.5 fs for the nuclear dynamics and a time step of 0.02 fs for the propagation of the electronic wavefunction, using the local diabatization formalism [75]. Energy conservation during a surface hop was ensured by scaling of the full velocity vectors, since the non-adiabatic coupling vectors are not available for our level of theory. We employed an energy-based decoherence correction with a parameter of 0.1 Hartree [76]. The initial geometries and velocities for the trajectories were sampled from a Wigner distribution of the harmonic ground state potential. In this way, 1000 geometries were produced and a single-point calculation at the MS-CASPT2(12,8) level of theory was

performed at each of these to obtain the state energies and oscillator strengths. The initial excited states were selected stochastically [77] restricting the excitation energy window between 4.775 - 4.825 eV. The ionization probability along the trajectories was obtained in an approximate manner from Dyson norm calculations [78] using our WFOverlap code [79] in a post-processing step. The necessary wavefunctions of the neutral and ionized molecule were obtained at steps of 2.5 fs along the precomputed trajectories from MS-CASPT2(12,8)/ano-rcc-vdzp or MS-CASPT2(11,8)/ano-rcc-vdzp calculations including altogether 5 singlets, 9 doublets, 4 triplets and 4 quartets as well as all possible SOCs.

### Uracil Calculation Details

The ground state of the biologically relevant tautomer of uracil was optimized at DFT level using the B3LYP functional and 6-31G(d) basis set using Gaussian09 package[80]. The frequencies and normal modes were calculated at the same level of theory. A sampling was performed using a harmonic oscillator Wigner distribution in Newton-X[62, 63] program to generate 500 initial conditions (nuclear coordinates and velocities) based on the optimized geometry and the normal modes from the previous calculation. The $S_1$ ($n\pi^*$) and $S_2$ ($\pi\pi^*$) excited states of uracil for the 500 geometries were calculated at both the complete active space self consistent field (CASSCF) and multi-reference configuration interaction with singles (MRCIS) levels using cc-pVDZ basis set with an active space of 12 electrons in 9 orbitals. Three states were averaged at the CASSCF level. The vertical excitation energies and oscillator strengths were used to calculate the absorption cross sections to simulate the first absorption band of uracil in both CASSCF and MRCIS methods. The temperature was considered to be 298 K. A Lorentzian line shape and a phenomenological broadening ($\delta$) value of 0.1 eV were employed. Fig. 9 shows the theoretical absorption spectra of uracil at both the CASSCF and MRCIS level.

We performed nonadiabatic excited state dynamics simulations using trajectory surface hopping in Newton-X on CASSCF(12,9)/cc-pVDZ and MRCIS/CASSCF(12,9)/cc-pVDZ potential energy surfaces calculated using the Columbus 7.0 package[66–68]. The experimentally measured first absorption peak for uracil in the gas-phase is at 5.08 eV[43]. The first absorption peak is at 6.60 eV and 5.90 eV for CASSCF and MRCIS levels, respectively. The pump-pulse generated in our experiment is at 4.77 eV which is 0.31 eV lower than the experimental maximum. So, 0.31 eV is subtracted from the peak of the theoretical spectra at both levels of theory to estimate the center of the pump pulse. The excitation windows were considered to be 6.29 ± 0.15 eV and 5.59 ± 0.15 eV at CASSCF and

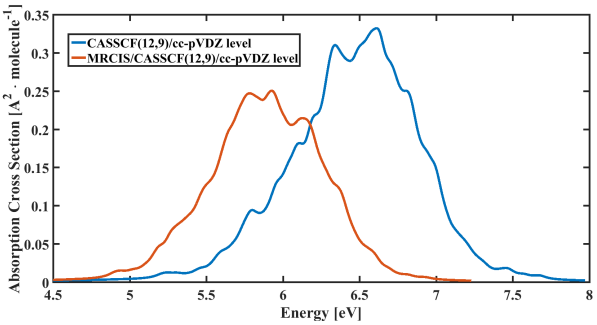


FIG. 9. Theoretical absorption spectra of uracil simulated at the CASSCF(12,9)/cc-pVDZ level (solid blue line centered around 6.5 eV) and MRCIS/CASSCF(12,9)/cc-pVDZ level (solid red line centered around 5.8 eV).

MRCIS level, respectively, selecting 71 and 73 initial conditions for the aforementioned levels of theory, to be propagated starting from the $S_2$ state as it is the first bright state in uracil. The fewest switches surface hopping (FSSH) algorithm was used to take into account non-adiabatic events between $S_2$, $S_1$ and $S_0$ states. The FSSH algorithm was corrected for decoherence effects using the approach of 'non-linear decay of mixing' by Zhu et al.[81] and Granucci et al.[76] keeping the parameter, $\alpha = 0.1$ Hartree. The velocity verlet algorithm was used to integrate Newtons equations of motion with a time step of 0.5 fs and the semi-classical Schrödinger equation was integrated using 5th order Butcher's algorithm with time step of 0.025 fs. The simulations were performed for 1000 fs at the CASSCF level and 500 fs at the MRCIS level using XSEDEs computational resources[82].

## APPENDIX III: EVIDENCE FOR PROBING EXCITED STATE DYNAMICS

We calculated the Frank Condon (FC) factors of the ground and the excited states in uracil in order to show that with our VUV-probe we can only ionize population in $S_1$ and $S_2$, and we cannot see any ionization from $S_0$, even if we assume we have a 'hot' ground state. This illustrates why a VUV-probe is needed in order to do a proper weak-field pump-probe experiment.

ezSpectrum 3.0 [83] was used to calculate FC overlaps using the Duschinsky rotations approximation. We define the FC factors as $|\langle\psi_{v_{\text{final}}}|\psi_{v_{\text{initial}}}\rangle|^2$, where $\psi_{v_{\text{initial}}}$ and $\psi_{v_{\text{final}}}$ are the initial and final vibrational states. The $S_0$ and $D_0$ minima were optimized at the B3LYP/6-31G(d) and UB3LYP/6-31G(d) level of theory, respectively. Frequencies and normal modes were calculated at the same level of theory and used for the FC overlap calculations. In order to obtain the correct character for the $D_1$ minimum we had to use TDDFT/TDA/CAM-B3LYP/6-31G(d) level, since the B3LYP functional did

not give the correct character. For consistency the $S_1$ minimum was also obtained at the same level of theory. Frequencies and normal modes were calculated at the TDDFT/TDA/CAM-B3LYP/6-31G(d) level of theory for the $S_1$ and $D_1$ minima and were used in the FC overlap calculations. The minima and normal modes were calculated with Q-Chem package [84].

FC factors were calculated between $S_0$ and $D_0$ and between $S_1$ and $D_1$. The results can be see in Fig. 10, where the UV and VUV-photon energies are also indicated. In Fig. 10 a) it is clear that the UV and VUV-photon energy are not energetically capable of ionizing from $S_0$ to $D_0$, even if the ground state were vibrationally hot. Fig. 10 b) shows the FC factors between $S_1$ and $D_1$ which indicate that the UV-photon energy is insufficient to ionize from $S_1$ without excess vibrational energy, making it a poor probe of $S_1$. In contrast, the VUV-photon has more than enough energy to ionize $S_1$ to $D_1$ from its lowest vibrational level, and is a good probe of $S_1$. The VUV-photon is in a unique position to enable us to fully probe any dynamics in $S_1$, but is still 'blind' to ground state dynamics.

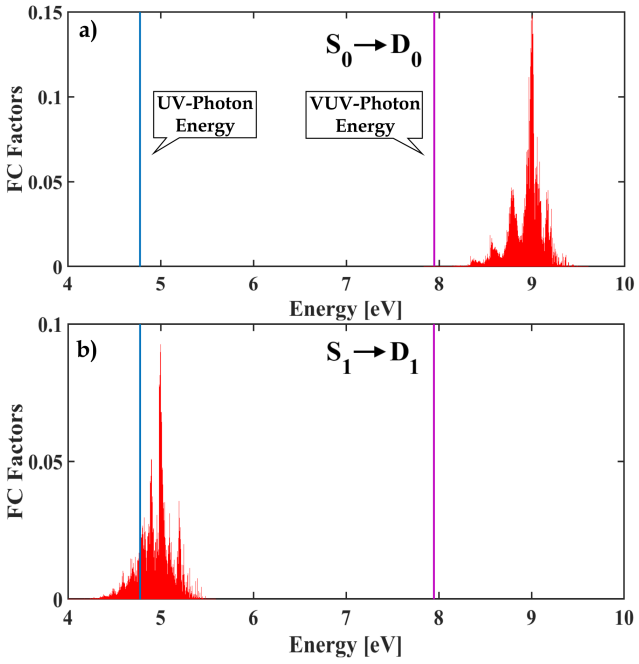


FIG. 10. FC Factors between a) $S_0$ and $D_0$ b) $S_1$ and $D_1$. The UV- and VUV-photon energies are labels and are indicated by the blue (4.8 eV) and magenta (7.95 eV) vertical lines respectively.